RSC Advances

PAPER

View Article Online
View Journal | View Issue

Cite this: *RSC Adv.*, 2020, **10**, 30776

Poly[2,2′-(4,4′-bipyridine)-5,5′-bibenzimidazole] functionalization of carbon black for improving the oxidation stability and oxygen reduction reaction of fuel cells†

Mohamed R. Berber *[ab] and Mohamad Y. Mustafa[c]

The rapid oxidation of carbon black (CB) is a major drawback for its use as a catalyst support in polymer electrolyte fuel cells. Here, we synthesize poly[2,2′-(4,4′-bipyridine)-5,5′-bibenzimidazole] (BiPyPBI) as a conducting polymer and use it to functionalize the surface of CB and homogenously anchor platinum metal nanoparticles (Pt-NPs) on a CB surface. The as-prepared materials were confirmed by different spectroscopic techniques, including nuclear magnetic resonance spectroscopy, energy-dispersive X-ray, thermal gravimetric analysis, and scanning-transmittance microscopy. The as-fabricated polymer-based CB catalyst showed an electrochemical surface area (ECSA) of 63.1 cm^2 mg_{Pt}^{-1}, giving a catalyst utilization efficiency of 74.3%. Notably, the BiPyPBI-based CB catalyst exhibited remarkable catalytic activity towards oxygen reduction reactions. The onset potential and the diffusion-limiting current density reached 0.66 V and 5.35 mA cm^{-2}, respectively. Furthermore, oxidation stability testing showed a loss of only 16% of Pt-ECSA for BiPyPBI-based CB compared to a 36% loss of Pt-ECSA for commercial Pt/CB after 5000 potential cycles. These improvements were related to the synergetic effect between the nitrogen-rich BiPyPBI polymer, which promoted the catalytic activity through the structural nitrogen atoms, and demolished the degradation of CB *via* the wrapping process.

Received 13th May 2020
Accepted 2nd August 2020

DOI: 10.1039/d0ra04289g

rsc.li/rsc-advances

Introduction

Polymer electrolyte fuel cells (PEFCs) are a sustainable power technology with massive potential for portable, automotive, and stationary power applications.[1] The performance and lifetime of PEFCs have been considered as the key constraints for the widespread application of this technology.[2] Accordingly, the components of PEFC units are gaining a lot of interest from both scientific and industrial perspectives.

The catalyst layer (CL) of PEFCs is one of the key components that strongly affect the performance and lifetime of PEFCs.[3] It usually consists of a carbon-support nanomaterial with a nanometal catalyst on which the FC reactions occur.[4] The performance degradation of the CL is typically caused by agglomeration, sintering, or the detachment of the nanometal catalyst due to the corrosion of the carbon-support nanomaterial.[5] Therefore, the design and surface-morphology of the CL are of great interest because they determine the catalyst utilization efficiency and also define how the protons and electrons transfer through the membrane electrode assembly (MEA). Carbon black (CB) is one of the most popular carbon-support materials in CL because it has a low production cost, a high specific surface area, and high electronic conductivity.[6] The main drawback of CB is its porous and amorphous structure, which contains a lot of oxygen-containing functional groups.[7] This structure leads CB to a fast oxidation process under the acidic operating conditions of FCs.[8] Thus, it is important to offer an advanced formulation route for CB into the CL to reach its optimum use in PEFCs.

The polymer modification of carbon supports showed remarkable impacts on the durability of CL and activity of the supported nanometal catalysts.[9] Numerous polymers including polytetrafluoroethylene (PTFE), perfluoro-sulfonic acid polymer (PFSA; Nafion), polypyrrole, and poly(ether–ether ketone) (PEEK) were introduced to the CL to improve its proton mobility, and to create contact between the CL and the membrane of the PEFCs. However, some of these polymers suffered from low stability under the harsh operating conditions of FCs, and the others could not meet the required targets for proton conductivity.[10,11] Therefore, there is a need for an ionomer that can provide high proton conductivity, high catalytic activity, and high stability of the nanometal catalyst as well

[a]*Chemistry Department, College of Science, Jouf University, Sakaka 2014, Saudi Arabia. E-mail: mrberber@ju.edu.sa*

[b]*Chemistry Department, Faculty of Science, Tanta University, Tanta 31527, Egypt. E-mail: mrberber@science.tanta.edu.eg*

[c]*Institute of Buildings, Energy and Material Technology, Faculty of Engineering Science and Technology, The Arctic University of Norway, Norway*

† Electronic supplementary information (ESI) available. See DOI: 10.1039/d0ra04289g

as low degradation of the carbon-supports. Polybenzimidazole-based (PBI) polymers are promising candidates for PEFCs that work at high operating temperatures and under non-humidifying conditions because they exhibit a high molecular weight, high thermal stability, good proton conductivity with a relatively lower production cost compared to other proton conducting ionomers. PBI polymers are predominantly introduced to PEFCs as proton conducting membranes in order to improve the proton mobility into the assembled MEA. Also, its aromatic structure is favored for the π–π interactions that occur with the surface of the carbon support materials. These interactions are advantageous for improving the catalyst stability at high operating temperatures.

Very recently, we offered a nitrogen-rich PBI polymer, namely poly[2,2′-(4,4′-bipyridine)-5,5′-bibenzimidazole] (BiPyPBI), with remarkable physicochemical properties owing to the nitrogen atoms of the polymer backbone.[12] In this study, we controlled the molecular weight of BiPyPBI to provide conducting membranes with high oxidative stability, high resistance towards thermal degradation, and improved proton conductivity. These properties allow BiPyPBI to be a promising ionomer for CLs.

In the current study, we use BiPyPBI as an ionomer to synthesize an advanced CL with improved performance and durability. BiPyPBI is envisioned to deaccelerate the oxidation stability of a CB catalyst-support through the wrapping of CB pores, and to work as an interfacial binder for the nanometal catalyst (platinum, Pt), forming a three-phase boundary structure (CB/BiPyPBI/Pt) with enhanced catalytic activity and durability. Typically, we investigate the oxygen reduction reaction (ORR), the electrochemical surface area (ECSA), the oxidative stability, and the degradation behaviour of the formed Pt/BiPyPBI/CB catalyst in comparison to the commercially available Pt/CB catalyst to show the impact of BiPyPBI on the CL.

Experimental

Materials

3,3′-Diaminobenzidine tetrahydrochloride, 2,2′-bipyridine-4,4′-dicarboxylic acid, chloroplatinic acid hexahydrate, polyphosphoric acid, *N*,*N*-dimethylacetamide, perchloric acid, and ethylene glycol were purchased from AlfaAesar Chemicals, Ltd. 2-Propanol, methanol, sodium hydroxide, and phosphoric acid were purchased from El-Gomhouria company for Trading Chemicals and Medical Appliances. CB (Vulcan XC-72R) was obtained from Cabot Chemicals, Ltd.

Synthesis of BiPyPBI

The BiPyPBI polymer was prepared by a condensation process according to our previous paper (see Fig. 1a).[12] Typically, equimolar ratios (60.0 mmol) of 3,3′-diaminobenizidine tetrahydrochloride and 2,2′-bipyridine-4,4′-dicarboxylic acid were added to a three-necked flask and mechanically mixed in 300 g of polyphosphoric acid at 200 °C for 36 h. The obtained polymer was then precipitated in hot water, washed with water, and rinsed with 10 wt% sodium hydroxide solution. The BiPyPBI was finally purified by hot methanol.

BiPyPBI wrapping of CB

First, 10 mg of the BiPyPBI polymer was added to 40 mL of *N*,*N*-dimethylacetamide, and then the mixture was thoroughly stirred at room temperature overnight to completely dissolve the BiPyPBI polymer. Next, 20 mg of CB was ultrasonically dispersed in 20 mL of *N*,*N*-dimethylacetamide for 30 min. After that, the BiPyPBI polymer and the dispersed CB solutions were mixed, sonicated for 30 min, and finally stirred at room temperature for 5 h to ensure the wrapping process. Subsequently, the obtained composite (donated as BiPyPBI/CB) was filtered, washed with *N*,*N*-dimethylacetamide several times to remove the unbound BiPyPBI polymer, and finally oven-dried at 80 °C overnight (see Fig. 1b). This synthetic process is assumed to ensure a monolayer coating of the polymer on the surface of CB.

Pt deposition on CB/BiPyPBI

The Pt nanoparticles (PtNPs) were deposited on the BiPyPBI/CB composite-support by a dispersion-seeding technique using chloroplatinic acid hexahydrate as the source of the Pt ions. Ethylene glycol was used as a reducing agent for the Pt ions.[13] Typically, 10 mg of the BiPyPBI/CB composite was ultrasonically dispersed in 100 mL of ethylene glycol aqueous solution for 30 min. For the Pt ions seeding, 0.85 mM of chloroplatinic acid hexahydrate was added and the resultant suspension was sonicated for 30 min, followed by a reflux process at 140 °C for 8 h to reduce the Pt ions. The formed Pt/BiPyPBI/CB catalyst was filtered, rinsed with water, and then acetone and finally, vacuum dried at 80 °C (see Fig. 1b).[13] Using the same process, Pt was deposited on CB.

Characterizations and measurements

The nuclear magnetic resonance (NMR) spectrum of the BiPyPBI polymer was measured using a Bruker 400 MHz (Bruker, Biospin AG) at Kafr Elsheikh University. The thermal behavior of the formed catalyst and the content of the Pt metal in the CL was determined (TGA) using a Shimadzu thermogravimetric analyzer (TGA-50). The TGA measurements were performed at a heating rate of 10 °C min^{-1} and an air flow rate of 20 mL min^{-1}. The size and distribution of PtNPs were analyzed using an ultra-high resolution scanning electron microscope (Hitachi-SU9000) equipped with an energy-dispersive X-ray detector (EDX), operated at 30 kV. The X-ray photoelectron spectroscopy was performed on an XPS from Thermo Scientific. The Brunauer–Emmett–Teller (BET) surface area was obtained from the N_2 adsorption–desorption isotherms measured at a −196 °C.

Molecular weight (MW) determination of the BiPyPBI polymer

The MW of BiPyPBI was measured by evaluating the inherent viscosity of BiPyPBI in the sulfuric acid solvent and[14,15] applying

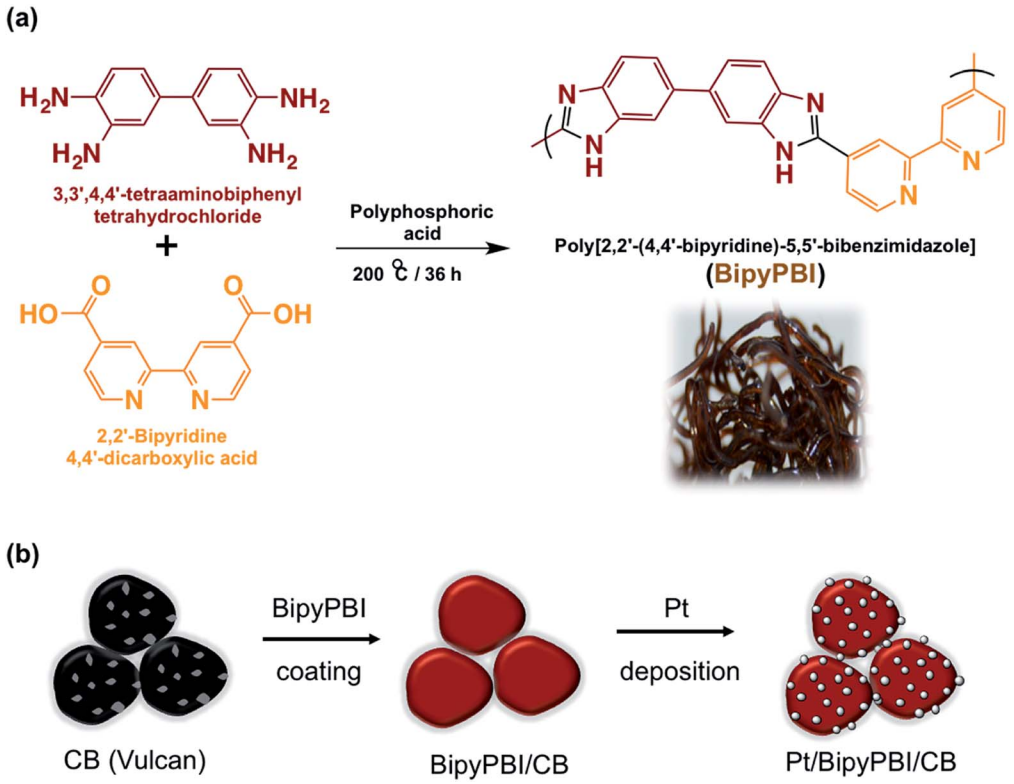

Fig. 1 Synthetic protocol for the (a) BiPyPBI polymer and (b) Pt/BiPyPBI/CB composite.

the Mark–Houwink–Sakurada equation.[16] The calculated MW was 139 kDa.

Electrochemical surface area (ECSA) and oxygen reduction reaction (ORR) measurements

The ECSA of PtNP was calculated by performing the cyclic voltammetry (CV) of the CL at room temperature in deoxygenated 0.1 M perchloric acid using a conventional three-electrode electrolytic cell connected with an ALS-potentiostat (Model DY2323). Typically, 14 μg cm^{-2} of PtNP was loaded onto the working electrode (which possesses a geometric surface area of 0.282 cm^2), while the counter and the reference electrodes were a Pt-wire and a Ag/AgCl system, respectively. The total catalyst loading on the working electrode was 43.75 μg and 38.88 μg for the commercially CB/Pt catalyst and the Pt/BiPyPBI/CB catalyst, respectively. The catalyst was deposited on the working electrode using a drop-cast/vacuum deposition process and a catalyst ink solution. No additional ionomer was added to the catalyst layers, which were composed of CB and Pt for commercial CB/Pt, and CB, BiPyPBI, and Pt for the Pt/BiPyPBI/CB systems. The cyclic voltammograms were collected at a scan rate of 50 mV s^{-1}. The ECSA values were calculated from the hydrogen adsorption region in the negative-going potential scan of the CVs.[17,18] The utilization efficiency of the Pt/BiPyPBI/CB catalyst was then determined to evaluate the preparation process of the catalyst in comparison to the commercial Pt/CB catalyst (see Table 1).[19] The specific surface area (SSA) was determined from the following equation. $SSA = 6 \times 1000/P \times d$, where P is the platinum density (21.4 g cm^{-3}), and d is the Pt particle size (nm).[19] The ORR activity was evaluated from the linear sweep voltammetry (LSV) measurements at 1600 rpm in an oxygen-saturated 0.1 M perchloric acid solution using a rotating disk electrode (RDE) at a scan rate of 10 mV s^{-1}. The RDE consisted of a glassy carbon disc surrounded by a layer of polytetrafluoroethylene.

Oxidative stability testing

The oxidative stability of the CL was tested in a deoxygenated 0.1 M perchloric acid solution at room temperature *via* an accelerated durability protocol provided by the Fuel Cell Commercialization Conference of Japan (FCCJ).[20] Typically, the durability was measured by potential cycling in the potential range from 1.0 to 1.5 V at a scan rate of 0.5 V s^{-1} for 5000 potential cycles. To see the effect of carbon corrosion on the CL stability, the ECSA of PtNPs was determined every 1000 cycles. Also, the CL after the durability test was investigated by ultra-high resolution scanning electron microscopy.

Results and discussion

Proton NMR confirmation of BiPyPBI structure

The ^{1}H-NMR signals were in accordance with the structure of BiPyPBI. Typically, the signals of BiPy-PBI were noted at δ (ppm) 13.26 (2H, s, N–H), 9.15–9.17 (2H, d, Ar-H), 8.3–8.33 (2H, d, Ar-H), 8.05 (2H, s, Ar-H), 7.85–7.9 (2H, d, Ar-H), 7.75 (2H, s, Ar-H), and 7.6–7.65 (2H, d, Ar-H).[12]

Table 1 Particle size, ECSA, specific surface area, utilization efficiency, and current–potential data for the Pt/BiPyPBI/CB and Pt/C catalysts

Sample name	Pt particle size (nm)	ECSA ($cm^2\ mg_{Pt}^{-1}$)	Specific surface area ($cm^2\ mg_{Pt}^{-1}$)	Utilization efficiency (%)	Onset potential (V *vs.* Ag/AgCl)	Limiting current density ($mA\ cm^{-2}$)
CB/BiPyPBI/Pt	3.3	63.1	84.9	74.3	0.66	−5.35
CB/Pt	3.0	65.2	93.4	69.8	0.62	−5.11

The composite structure of Pt/BiPyPBI/CB

The XPS surface analysis was performed to confirm the BiPyPBI surface coating of CB. Fig. S1† shows the XPS survey scan of the BiPyPBI/CB composite. The XPS spectrum shows the characteristic N_{1s} and C_{1s} signals of BiPyPBI and CB, respectively. The N/C ratio, determined from the XPS spectrum, was 3/97. This indicated a very small loading ratio of the BiPyPBI polymer and supports the monolayer nature of the BiPyPBI coating.

EDX spectroscopy was used to confirm the composite structure of Pt/BiPyPBI/CB. As expected, the EDX result showed the spectral peaks of the Pt, N, and C elements (Fig. 2a), which are characteristic for the Pt-metal catalyst, BiPyPBI polymer, and CB of the composite, respectively. The peak of the O element was due to the oxygen-functional groups of CB. As proposed, the π–π and CH–π interaction forces were in charge of the interactions between BiPyPBI and the CB surface.[21] Also, coordination bonding was responsible for the binding of the Pt metal ions on the surface of the BiPyPBI/CB composite.[22] Besides, the transmission image and the surface image of the composite (Fig. 2b and c) showed the Pt metal as bright and dark nanoparticles spots, evenly distributed with no aggregates on the surface of BiPyPBI/CB. The particle size distribution histogram (Fig. 2d) indicated the formation of PtNPs with an average size of 3.3 nm. The transmission and surface images of the commercial Pt/CB composite also showed Pt-NPs with an average size of 3.0 nm, homogenously distributed on the surface of CB (see Fig. 3).

TGA was performed to evaluate the effect of the BiPyPBI polymer on the thermal behavior of the assembled composite and was also used to determine the loading ratio of the Pt metal catalyst. Fig. 4a shows the thermal behavior of CB. As seen, the thermal decomposition temperature of CB was around 700 °C. The commercial Pt/CB catalyst (Fig. 4b) showed a much lower decomposition temperature of around 398 °C due to the catalytic activity of the loaded Pt metal catalyst, which promoted the thermal degradation of carbon.[23,24] As observed, the Pt loading ratio in the Pt/CB composite was 32%. On the other side, the Pt/BiPyPBI/CB composite showed an enhanced thermal behavior compared to that of Pt/CB (Fig. 4c). The decomposition temperature of CB in the Pt/BiPyPBI/CB composite was recorded at 450 °C (around 52 °C higher than that of CB in Pt/CB). This improvement was correlated to the BiPyPBI polymer, which has high thermal stability with a decomposition temperature of 600 °C (see Fig. S2†). The BiPyPBI polymer in the Pt/BiPyPBI/CB composite worked as a protective layer, blocking the active oxidation sites of CB, and accordingly raised the activation energy required for the thermal decomposition of CB.[25] Notably, there was a decrease in temperature at around 460 °C. This behavior was related to the heat absorbed by CB during its rapid decomposition process,[26] resulting in the cooling down of its surroundings. When the oxidation of CB was complete, the composite temperature increased and then thermalized with the TGA apparatus temperature. In addition, there was a small weight loss of 3% at around 500 °C. This weight loss was related to the amount of BiPyPBI in the composite.[12]

ECSA and ORR performance

Fig. 5a shows the cyclic voltammograms of both Pt/BiPyPBI/CB (red curve) and Pt/CB (black curve) CLs. As seen, the cyclic voltammograms of both CLs display identical peak shape and position for hydrogen adsorption and desorption on the surface of Pt in the low potential region as well as the Pt reduction and oxidation position in the high potential region.[27] The initial ECSAs calculated from the hydrogen adsorption region in the negative-going potential scan of the cyclic voltammograms were 63.1 and 65.2 $cm^2\ mg_{Pt}^{-1}$ for Pt/BiPyPBI/CB and Pt/CB, respectively. The slight decrease in the ECSA of Pt/BiPyPBI/CB was due to the slight increase in the Pt particle size, as confirmed by the TEM images. In addition, and as seen from the data in Table 1, the Pt specific surface area of Pt/BiPyPBI/CB was 84.9 $cm^2\ mg_{Pt}^{-1}$ compared to 93.4 $cm^2\ mg_{Pt}^{-1}$ for the commercial Pt/CB catalyst, giving utilization efficiencies of 74.3% and 69.8%, respectively. This improvement in the utilization efficiency of Pt/BiPyPBI/CB was related to the BiPyPBI polymer, which partially covered the surface pores of the CB support, preventing the Pt-NPs from impeding into the pores of CB. The nitrogen-gas adsorption/desorption measurements of CB before and after BiPyPBI wrapping (Fig. S3†) confirmed this hypothesis. The calculated BET surface area was 181 $m^2\ g^{-1}$ for CB and became 91 after BiPyPBI polymer wrapping (see Table 2). In addition, the pore volume of CB decreased by a ratio of 86% as a result of the BiPyPBI polymer filling of CB pores (see Fig. S4,† and Table 2). Fig. 5b shows the polarization curves of Pt/BiPyPBI/CB in comparison to Pt/CB. When comparing the onset potential and the diffusion-limiting current density, Pt/BiPyPBI/CB exhibited a higher ORR activity compared to Pt/CB (see Table 1). The onset potential and the diffusion-limiting current density of Pt/BiPyPBI/CB reached 0.66 V and 5.35 $mA\ cm^{-2}$, respectively. These improvements were due to the synergetic effect of the nitrogen-based BiPyPBI, which promoted ORR through the nitrogen atoms of the BiPyPBI backbone.[28]

In order to show the impact of BiPyPBI on the oxidation stability of CB, potential-stress testing was performed. Fig. 6a and b show the cycling voltammograms (CV) of Pt/BiPyPBI/CB

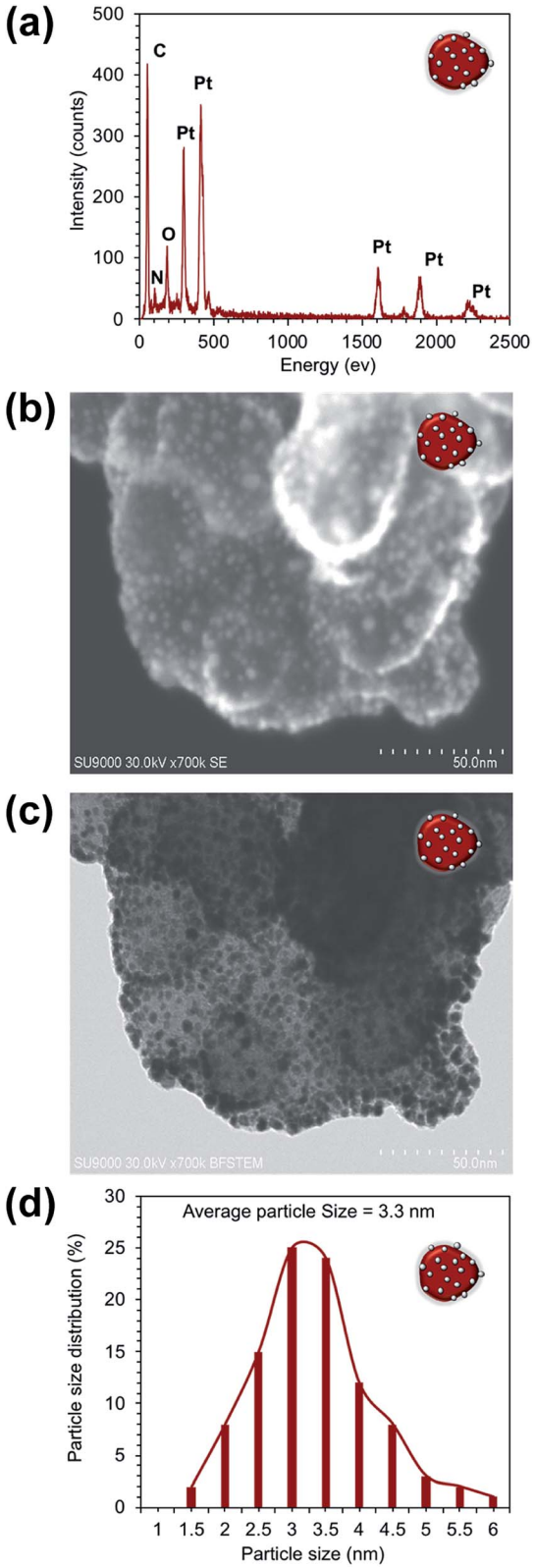

Fig. 2 (a) Energy dispersive X-ray (EDX) spectrum of the Pt/BiPyPBI/CB composite. STEM images of the Pt/BiPyPBI/CB composite: (b) surface image, and (c) transmission image. (d) Particle size distribution histogram of Pt-NPs supported on the BiPyPBI/CB composite.

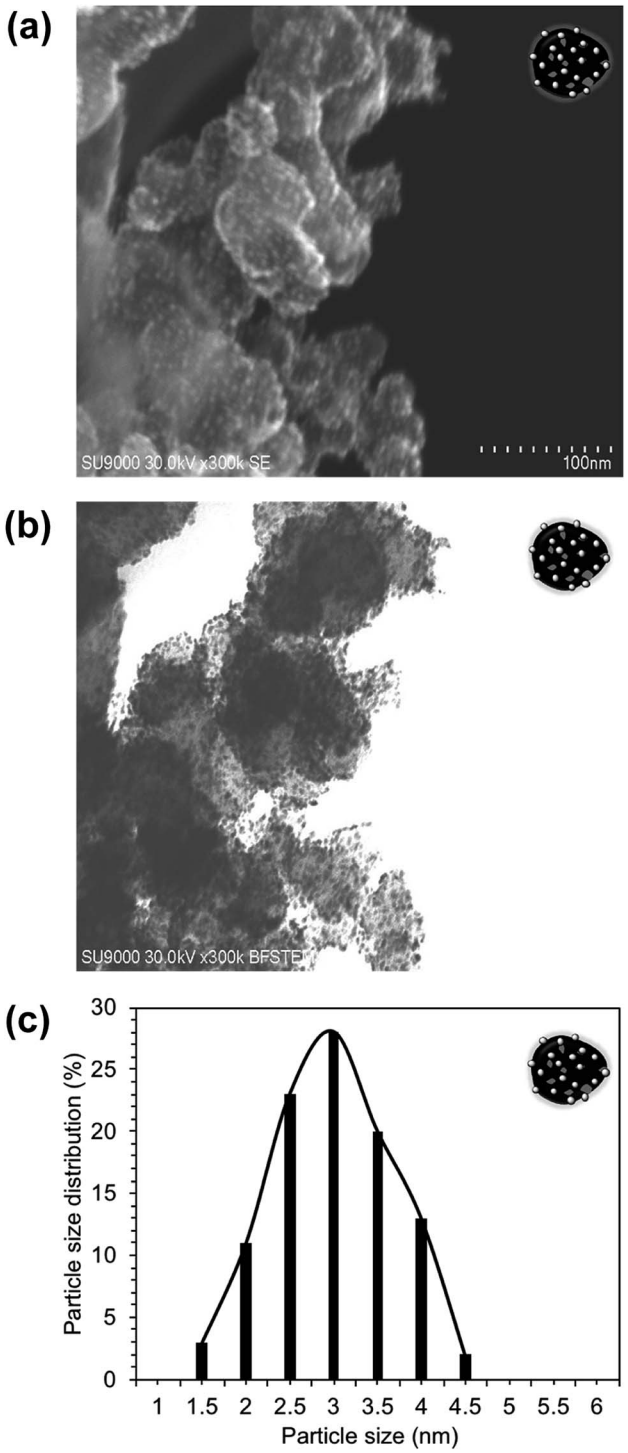

Fig. 3 STEM images of the Pt/CB composite: (a) surface image, and (b) transmission image. (c) Particle size distribution histogram of the Pt-NPs supported on CB.

and Pt/CB catalysts, respectively, before and after the potential-stress testing. When comparing the CV profiles, a massive decrease in the current density of Pt/CB was noticed compared to that of the Pt/BiPyPBI/CB catalyst after durability testing. This performance was related to the loss of the ECSA of the Pt metal catalyst. High ECSA loss results in a large drop in the current

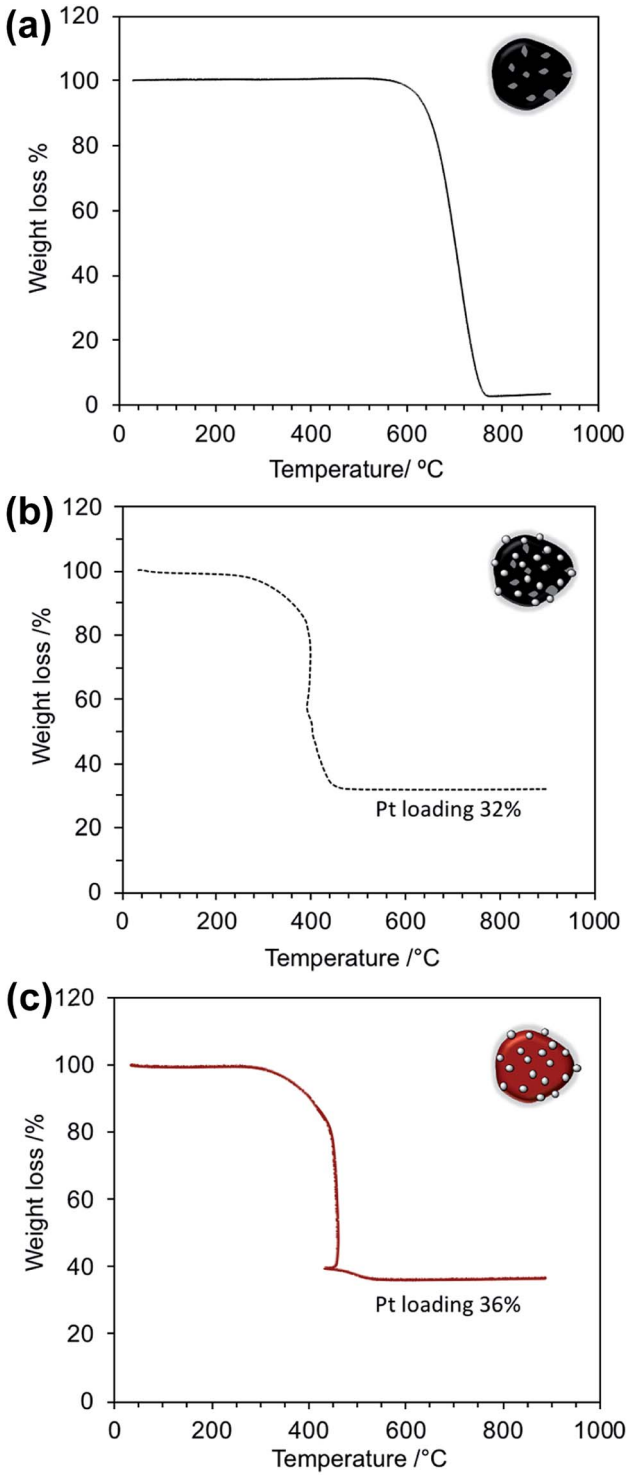

Fig. 4 TGA of: (a) CB, (b) the Pt/CB composite, and (c) the BiPyPBI/CB composite.

density.[29] This observation clearly showed how important the BiPyPBI coating is as it suspended the aging process of the CB that is responsible for the sintering of Pt and the loss of the ECSA. To clarify the variation in the ECSA during durability testing, the normalized-ECSAs are plotted against the number of potential cycling, as displayed in Fig. 6c. As observed, the

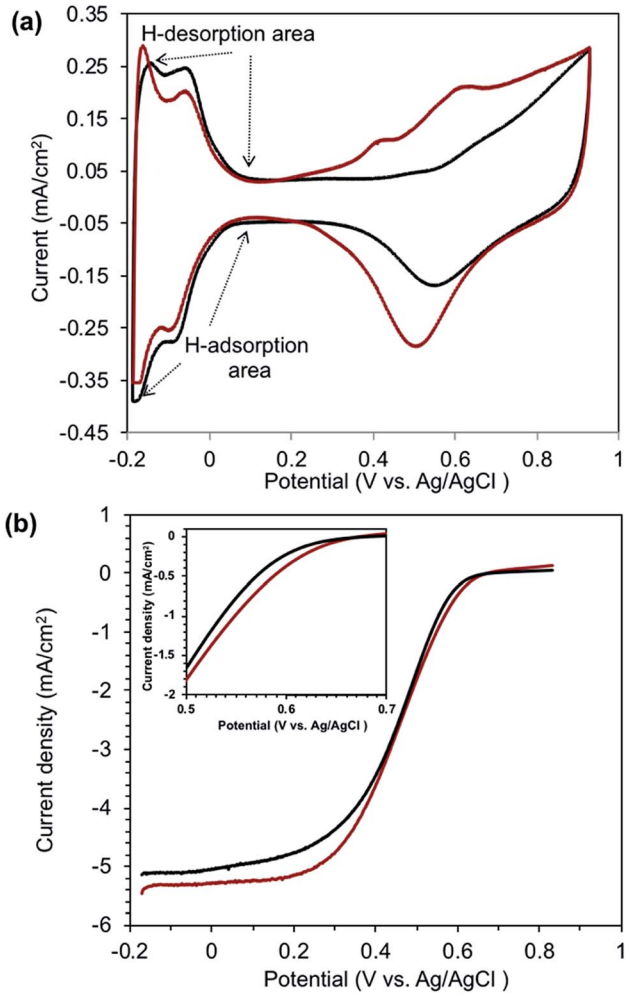

Fig. 5 Cyclic voltammograms (a), and polarization curves (b) of the Pt/BiPyPBI/CB (red curves) and Pt/CB (black curves) systems.

ECSAs of both the Pt/BiPyPBI/CB and Pt/CB catalysts decreased with increasing potential cycling. After 5000 cycles, a loss of only 16% of the initial Pt-ECSA of Pt/BiPyPBI/CB was observed compared to a 36%-loss for Pt/CB. The delay in the ECSA loss upon potential cycling of Pt/BiPyPBI/CB suggests outstanding electrochemical stability against corrosion. This delay in the degradation of the Pt/BiPyPBI/CB catalyst highlights the impact of wrapping CB with BiPyPBI.

To gain a better understanding of the degradation performance of both catalysts, STEM images (surface and transmittance) were captured after the durability tests (see Fig. 7 and

Table 2 BET surface area and pore volume of the BiPyPBI/CB and CB systems

Sample	BET ($m^2\ g^{-1}$)	Average pore volume ($cm^3\ Å^{-1}\ g^{-1}$)
CB	181	0.022
BiPyPBI/CB	92	0.003

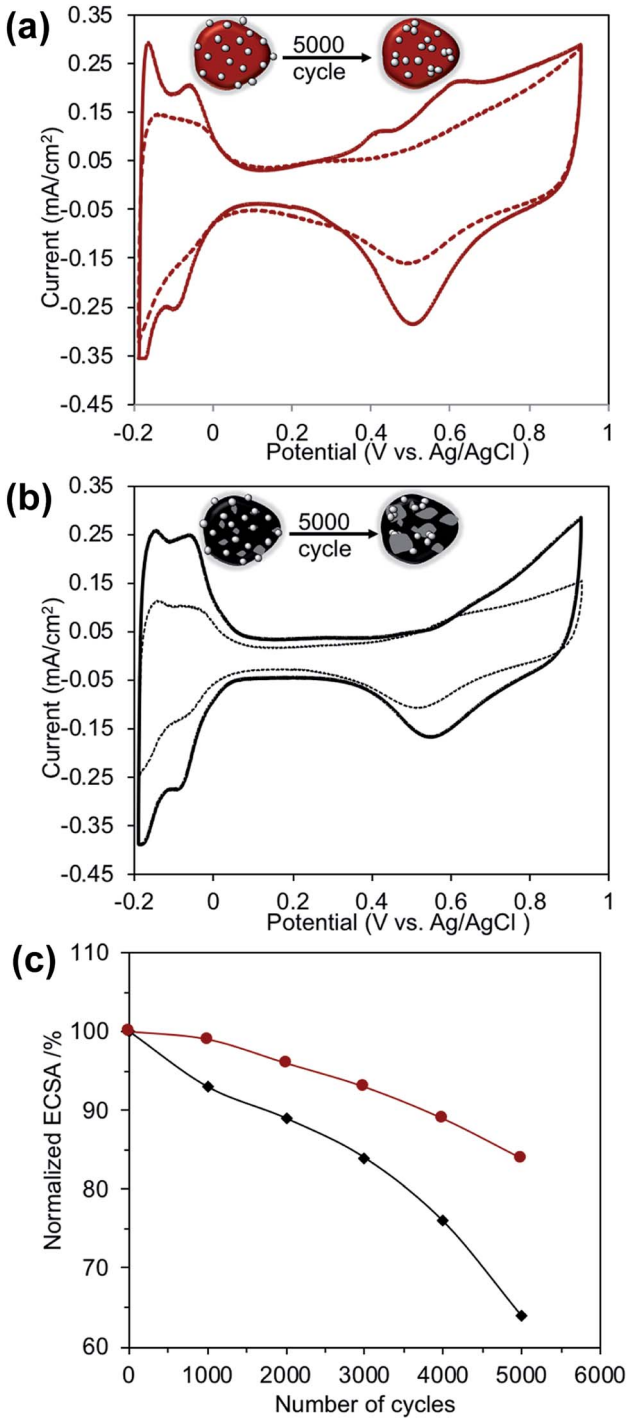

Fig. 6 Cyclic voltammograms of the: (a) Pt/BiPyPBI/CB catalyst and (b) Pt/CB catalyst, before (solid lines) and after (dashed lines) durability testing. (c) ECSA dependence of potential-cycling.

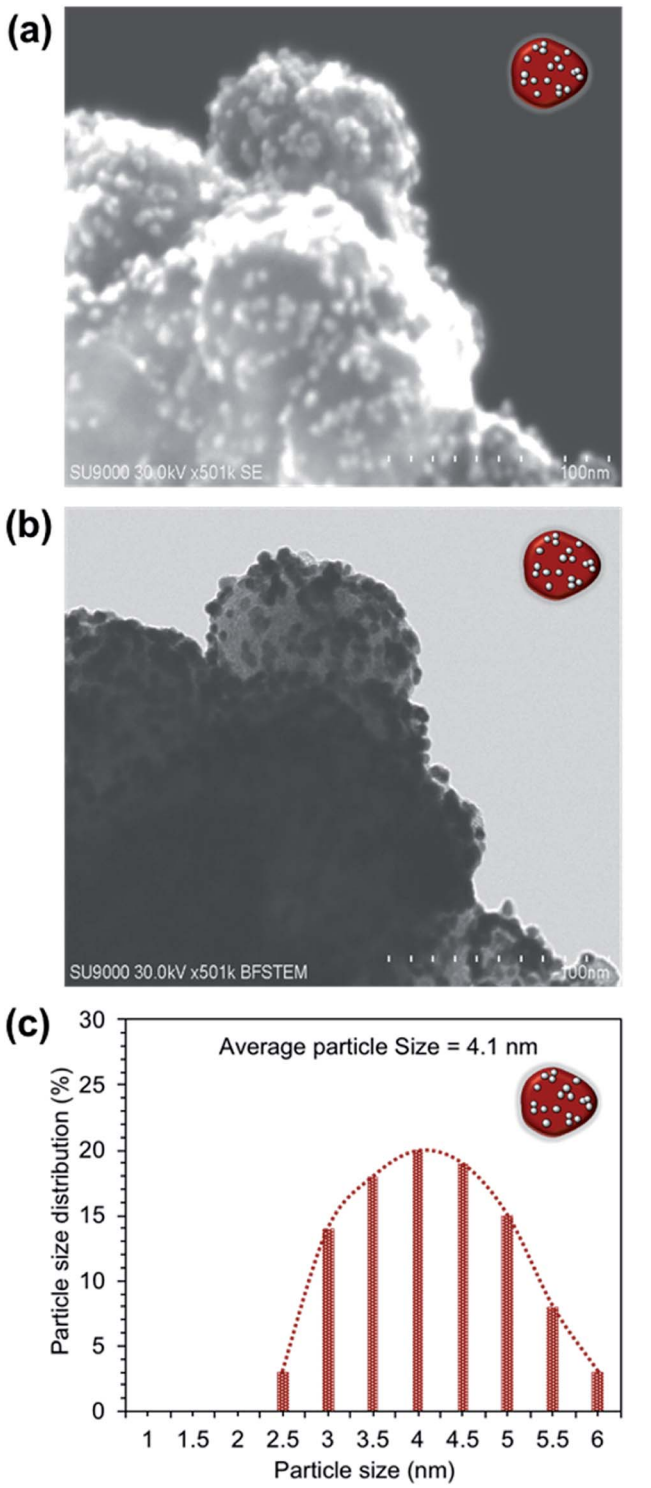

Fig. 7 STEM images of the Pt/BiPyPBI/CB composite after 500 potential-cycles: (a) surface image and (b) transmittance image. (c) Particle size distribution histogram of the Pt-NPs.

8). As seen, the Pt-NPs sintered and agglomerated in both catalysts.[30] The rate of sintering was high in the case of Pt/CB compared to the Pt/BiPyPBI/CB catalyst, resulting in larger Pt-NPs, as determined by the particle size histograms in Fig. 7c and 8c. In addition, and as noticed from the dark STEM images (Fig. 7a and 8a), the number of Pt-NPs left on the surface of the CB-support was low in the case of the Pt/CB composite compared to the Pt/BiPyPBI/CB composite, reflecting a loss of many active Pt-NPs in the case of the Pt/CB catalyst. The bright field images (Fig. 7b and 8b) indicated the presence of these Pt-NPs inside the CB support. These observations clearly indicate a higher corrosion process in the case of the Pt/CB catalyst, and

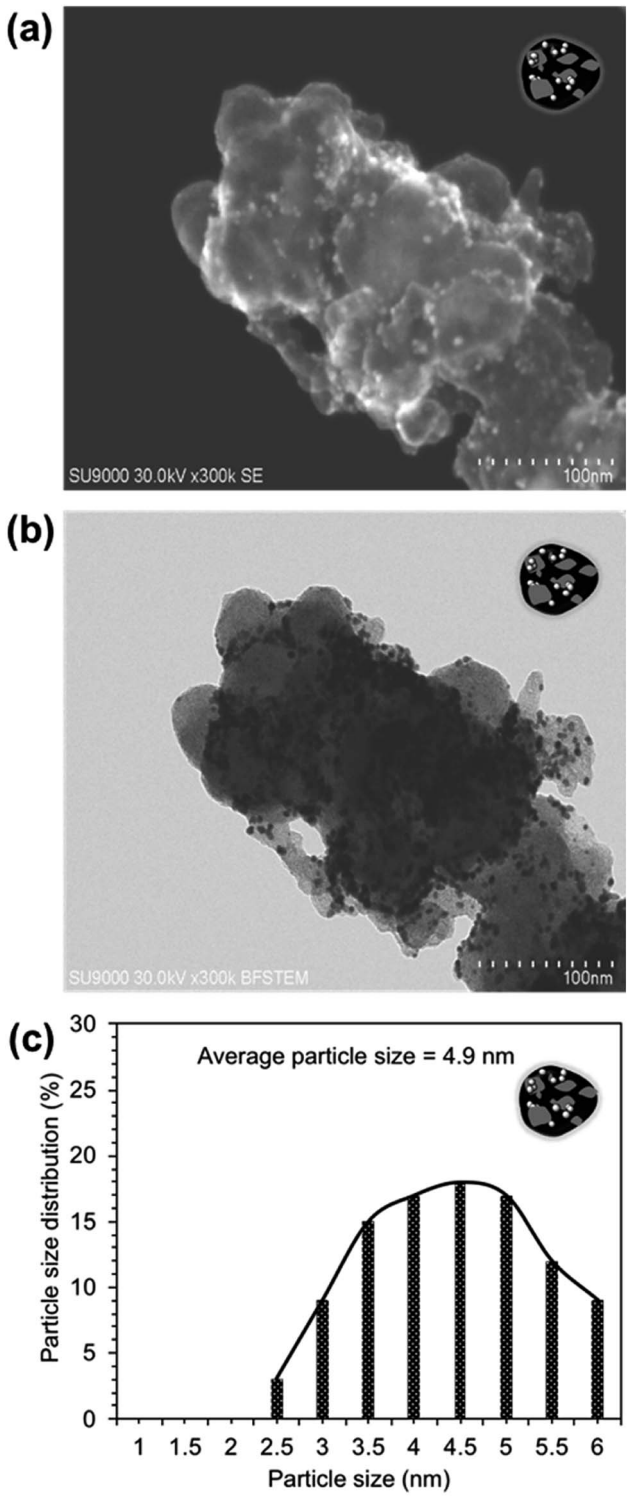

Fig. 8 STEM images of the Pt/CB composite after 500 potential-cycles: (a) surface image and (b) transmittance image. (c) Particle size distribution histogram of the Pt-NPs.

consequently a faster loss of in catalytic activity towards ORR. Based on these results, it became clear that BiPyPBI played a significant role in improving the electrochemical stability of CB, leading to higher durability against corrosion and accordingly a lower loss of Pt-ECSA. The BiPyPBI wrapping process and the BiPyPBI nitrogen-rich chemical structure strongly contributed to capturing and preventing the Pt-NPs from embedding into the pores of CB, keeping them stable on the surface.

Conclusion

A BiPyPBI conducting polymer was synthesized and used to functionalize the surface of CB. The formed BiPyPBI/CB composite showed homogenous loading of the Pt-NPs. The Pt-NPs had an average size of 3.3 nm with an ECSA of 63.1, which is comparable to the ECSA of the Pt/CB catalyst. The Pt specific surface area of Pt/BiPyPBI/CB reached 84.9 $cm^2\ mg_{Pt}^{-1}$ compared to 93.4 $cm^2\ mg_{Pt}^{-1}$ for the Pt/CB catalyst. The utilization efficiencies were 74.3% and 69.8%, respectively. In comparison to Pt/CB, Pt/BiPyPBI/CB showed improved catalytic activity towards ORR. This improvement in the catalytic activity was due to the synergetic effect between the nitrogen-based BiPyPBI, which promoted ORR through the nitrogen atoms of the BiPyPBI backbone. A loss of only 16% of initial Pt-ECSA of Pt/BiPyPBI/CB was recorded after 5000 potential cycles compared to a 36% loss for Pt/CB. This delay in the degradation of the Pt/BiPyPBI/CB catalyst highlighted the impact of wrapping CB with BiPyPBI. The electron microscopy investigations of the catalysts after durability testing indicated a higher corrosion rate for Pt/CB, and consequently, confirmed the faster ECSA loss of the Pt/CB catalyst. In general, the BiPyPBI wrapping of CB and the nitrogen-rich chemical structure of BiPyPBI are advantageous for improving both the catalytic activity towards ORR and the oxidation stability that prevents corrosion.

Data availability

The author confirms that the data supporting the findings of this study are available within the article.

Authors contributions

Mohamed R. Berber (MRB) proposed the research idea and designed the research experiments. MRB synthesized the polymer and the composite materials. MRB and Mohamad Y. Mustafa (MYM) analysed and characterized the materials. MRB and MYM shared the writing of the manuscript.

Conflicts of interest

There are no conflicts of interest to declare.

Acknowledgements

The Deanship of Scientific Research at Jouf University Funded this research through the Fast-track Research Funding Program; the authors are so grateful.

References

1 Y. Wang, K. S. Chen, J. Mishler, S. C. Cho and X. C. Adroher, *Appl. Energy*, 2011, **88**, 981–1007.
2 Z. Yang, M. R. Berber and N. Nakashima, *Electrochim. Acta*, 2015, **170**, 1–8.
3 M. Uchida, *Curr. Opin. Electrochem.*, 2020, **21**, 209–218.
4 J. Ko and H. Ju, *Int. J. Hydrogen Energy*, 2013, **38**, 682–691.
5 S. Sui, X. Wang, X. Zhou, Y. Su, S. Riffat and C.-j. Liu, *J. Mater. Chem. A*, 2017, **5**, 1808–1825.
6 S. Samad, K. S. Loh, W. Y. Wong, T. K. Lee, J. Sunarso, S. T. Chong and W. R. Wan Daud, *Int. J. Hydrogen Energy*, 2018, **43**, 7823–7854.
7 G. Inoue and M. Kawase, *J. Power Sources*, 2016, **327**, 1–10.
8 S. Takenaka, M. Goto, Y. Masuda, S. Emura and M. Kishida, *Int. J. Hydrogen Energy*, 2018, **43**, 7473–7482.
9 Y.-J. Wang, B. Fang, H. Li, X. T. Bi and H. Wang, *Prog. Mater. Sci.*, 2016, **82**, 445–498.
10 X. Cheng, B. Yi, M. Han, J. Zhang, Y. Qiao and J. Yu, *J. Power Sources*, 1999, **79**, 75–81.
11 A. Manthiram, X. Zhao and W. Li, in *Functional Materials for Sustainable Energy Applications*, ed. J. A. Kilner, S. J. Skinner, S. J. C. Irvine and P. P. Edwards, Woodhead Publishing, 2012, pp. 312–369, DOI: 10.1533/9780857096371.3.312.
12 M. R. Berber and N. Nakashima, *J. Membr. Sci.*, 2019, **591**, 117354.
13 M. R. Berber, T. Fujigaya and N. Nakashima, *Materials Today Energy*, 2018, **10**, 161–168.
14 A. M. R. Caparros and M. Bohdanecký, *Die Makromolekulare Chem.*, 1985, **186**, 1005–1013.
15 R. Pamies, J. G. Hernández Cifre, M. del Carmen López Martínez and J. García de la Torre, *Colloid Polym. Sci.*, 2008, **286**, 1223–1231.
16 Y. Yuan, F. Johnson and I. Cabasso, *J. Appl. Polym. Sci.*, 2009, **112**, 3436–3441.
17 D. V. Dao, G. Adilbish, T. D. Le, I.-H. Lee and Y.-T. Yu, *RSC Adv.*, 2019, **9**, 15635–15641.
18 T. Binninger, E. Fabbri, R. Kötz and T. J. Schmidt, *J. Electrochem. Soc.*, 2014, **161**, H121–H128.
19 T. Vidaković, M. Christov and K. Sundmacher, *J. Appl. Electrochem.*, 2009, **39**, 213–225.
20 A. Ohma, K. Shinohara, A. Iiyama, T. Yoshida and A. Daimaru, *ECS Trans.*, 2011, **41**, 775–784.
21 T. Kar, H. F. Bettinger, S. Scheiner and A. K. Roy, *J. Phys. Chem. C*, 2008, **112**, 20070–20075.
22 I. H. Hafez, M. R. Berber, T. Fujigaya and N. Nakashima, *ChemCatChem*, 2017, **9**, 4282–4286.
23 J. P. A. Neeft, M. Makkee and J. A. Moulijn, *Fuel*, 1998, **77**, 111–119.
24 E. Saab, S. Aouad, E. Abi-Aad, M. N. Bokova, E. A. Zhilinskaya and A. Aboukaïs, *Kinet. Catal.*, 2007, **48**, 841–846.
25 O. A. Baturina, S. R. Aubuchon and K. J. Wynne, *Chem. Mater.*, 2006, **18**, 1498–1504.
26 Y. Qiu, F. Collin, R. H. Hurt and I. Külaots, *Carbon*, 2016, **96**, 20–28.
27 Y. Wang, L. Zhang, M. Zhang and F. Li, *J. Mater. Chem.*, 2012, **22**, 12313–12318.
28 M. Li, X. Bo, Y. Zhang, C. Han, A. Nsabimana and L. Guo, *J. Mater. Chem. A*, 2014, **2**, 11672–11682.
29 C. A. Rice, P. Urchaga, A. O. Pistono, B. W. McFerrin, B. T. McComb and J. Hu, *J. Electrochem. Soc.*, 2015, **162**, F1175–F1180.
30 O. L. Li, Z. Shi, H. Lee and T. Ishizaki, *Sci. Rep.*, 2019, **9**, 12704.